Arabian Journal of Chemistry (2023) **16**, 105076

King Saud University

Arabian Journal of Chemistry

www.ksu.edu.sa
www.sciencedirect.com

ORIGINAL ARTICLE

Therapeutic potential of a triazole curcumin in inflammation: Decreased LPS-induced acute lung injury in mice by targeting MD2/TLR4

He WeiGang [a], Liu KaiQiang [a], Hou XueYou [a], Xu JiaHan [a], Zhi TaiXin [a], Deng YingKai [a], Hu JunYi [a], Jin MoYan [a], Wang JiaChen [a], Wang Xin [b], Sun XianYu [a,*]

[a] *School of Biology and Food Engineering, Changshu Institute of Technology, Changshu 215500, Jiangsu, China*
[b] *College of Animal Science and Technique, Heilongjiang Bayi Agriculture University, Daqing 163319, Heilongjiang, China*

Received 29 January 2023; accepted 10 June 2023
Available online 16 June 2023

KEYWORDS

Triazole Curcumin;
Acute Lung Injure;
MD2-TLR4;
NF-κB;
MyD88

Abstract Curcumin has a wide range of biological activities. This study investigated the anti-inflammatory activity of a triazole curcumin derivative (TAC)—especially its effect on lipopolysaccharide (LPS)-induced acute lung injury (ALI) in mice and possible targets. In the xylene-induced ear edema experiment, the inhibition rate of TAC against mice ear edema was 23.8%–78.2% over a dose range of 2.5–40 mg/kg 4 h after administration. At a dose of 10 mg/kg, the anti-inflammatory activity of TAC reached a peak at 4 h with an inhibition rate of 73.1%. This was significantly better than the positive control drug sodium diclofenac (DCF). TAC can also effectively reduce the degree of pulmonary edema injury in mice. H&E and Masson staining showed that the inflammatory and pathological indicators of LPS-induced lung injury were significantly improved by TAC. MTT tests illustrated that TAC showed weak cytotoxicity against RAW264.7 cells, and inhibited TNF-α and IL-6 release induced by LPS. Western blotting indicated that TAC decreased the expression of NF-κB and AP-1 in LPS pre-treated RAW264.7 cells, but failed to influence the expression of NF-κB in IL-1β pre-treated HET293T-Myd88$^{-/-}$ cells. Docking studies show that TAC could bind to the hydrophobic pocket of the CD2-TLR4 complex and expressed a high binding affinity. In conclusion, TAC exerts its anti-inflammatory effects by targeting the MD2-TLR4 signaling pathway, thus suggesting that it may be a promising candidate for the treatment of acute lung injury.

* Corresponding author.
E-mail address: sunxy@cslg.edu.cn (S. XianYu).
Peer review under responsibility of King Saud University.

Production and hosting by Elsevier

https://doi.org/10.1016/j.arabjc.2023.105076
1878-5352

1. Introduction

Uncontrolled inflammation is a key factor in the pathogenesis of various acute and chronic diseases, such as COVID-19 (Panoskaltsis, et al. 2021; Michels, et al. 2021). Acute lung injury (ALI) is a typical feature of patients with severe COVID-19 infection, which triggers an extreme immune response known as a "cytokine storm" (Coperchini, et al. 2021; Leist, et al. 2020). Thus, studying ALI in patients with COVID-19 can deepen our understanding of cytokine storms and improve disease prognosis. Current diagnosis and treatment guidelines for COVID-19 recommend glucocorticoids for patients with severe pneumonia; however, high-dose corticosteroids may lead to prolonged hospitalization, superinfection, and risk of various potential sequelae (Deng 2020). Therefore, developing a safe and effective drug for ALI treatment is a clinical priority.

ALI is a life-threatening clinical disease in critically ill patients. It is characterized by a strong inflammatory response in the lungs (Wang, et al. 2019). It is a diffuse inflammatory reaction in the lungs caused by various pathogenic factors inside and outside the lungs, and it is clinically characterized by respiratory distress and refractory hypoxemia followed by respiratory failure (Hughes and Beasley 2017). It is currently the main cause of death in critically ill patients. Adrenal silver glucocorticoids can be used for a short period of 1–2 days when ALI is life-threatening, but routine use is not recommended (Cepkova and Matthay 2006; Tu, et al. 2017). Non-cortisol anti-inflammatory drugs such as ibuprofen and sodium diclofenac (DCF) are used in the early stage of ALI and show a certain therapeutic effect (Niitsu, et al. 2011).

Curcumin is a natural product with symmetrical polyphenol structure isolated from the spice turmeric. Its anti-inflammatory and antioxidant activity has been demonstrated in numerous clinical trials and multiple indications (Nelson, et al. 2017; Kocaadam and Şanlier 2017). However, curcumin is limited in its medicinal effect due to its poor *in vitro* stability as well as unsatisfactory *in vivo* pharmacokinetic and pharmacodynamic properties (Campbell, et al. 2021). Thus, most of the reported structural modification work focused on changing the parent structure to develop curcumin analogs with improved stability, efficacy, and potency while retaining parent structure safety characteristics (Tang, et al. 2022; Wang, et al. 2015; Zhang, et al. 2018). A previous structural study *in vivo* indicated that curcumin rapid metabolism was predominantly caused by the methylene between 1,3-diketones, which has a strong nucleophilic activity and can effectively combine with drug-metabolizing metalloenzymes (Caprioglio, et al. 2016). Therefore, we introduced 1,2,3-triazole into the active methylene of 1,3-dione and found that a triazole curcumin (TAC, Fig. 1) suppressed lung cancer cell proliferation by inhibiting NF-κB/STAT3 signaling pathways (Zhi, et al. 2022). Moreover, considering the inextricable link between tumors and inflammation, we want to investigate the anti-inflammation activities of TAC and test its therapeutic potential in ALI while also evaluating its possible mechanism of action.

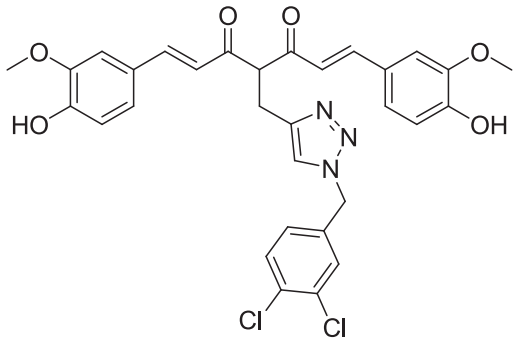

Fig. 1 Structure of TAC.

2. Materials and methods

2.1. Agents, animals, and cell culture

TAC was synthesized in our laboratory (Chemical biology Research Center, Changshu Institute of Technology). Starting material 3,4-dichloro benzyl bromide reacted with sodium azide to yield benzyl azide, which reacted with propiolic alcohol, the triazole alcohol intermediate was chlorinated and reacted with acetylacetone, finally condensed with vanillin in the presence of tributyl borate and boric anhydride (Zhi, et al. 2022). In cell experiments, TAC and the positive control DCF (JK scientific, China) were solubilized in DMSO and diluted with cell culture medium at an initial concentration of 100 μM with DMSO concentrations below 2% in all cell experiments. In animal experiments, TAC and the positive control drug DCF for oral administration were suspended in 0.5% carboxymethylcellulose sodium (CMC-Na) (Bian, et al. 2021).

RAW264.7 macrophages (China Cell Line Bank) were cultured in RPMI 1640 medium containing 10% fetal bovine serum and 1% penicillin/streptomycin. MYD88 knockout HEK293T cells ($Myd^{-/-}$, Beyotime, China) were cultured in DMEM containing 10% fetal bovine serum and 1% penicillin/streptomycin. Both cells were cultured in a 5% CO_2 humidified incubator at 37 °C. The cells grew adherently, and the culture medium was changed every two days.

Male Kunming mice weighing 20–22 g were purchased from the Laboratory Animal Center of Nantong University. The animals were fed a standard diet and water for at least 3 days prior to the start of the experiment. They were fasted for 2 h before administration and given free drinking water. Animal care and experimental procedures were approved by the Animal Policy and Welfare Committee of Changshu Institute of Technology (Changshu, China).

2.2. Mice ear edema model

Mice were orally administered TAC or DCF. After 30 min, 20 μL of xylene was evenly smeared on the front and back of the right ear. Mice were euthanized with ketamine after a certain time, both ears were cut off, and the same part of both ears was removed with a 7 mm punch and weighed. The weight of the right ear piece minus the weight of the left ear piece indicated the degree of edema, and the anti-inflammatory inhibition rate = 1−(edema degree/weight of the left ear piece) (Khan, et al. 2021).

2.3. Lipopolysaccharide (LPS)-induced acute lung injury in mice

Mice were orally administered TAC or DCF, and LPS (5 mg/kg) was instilled in the trachea 2 h after administration. Mice were euthanized with ketamine 6 h later (Xiao, et al. 2020).

Pulmonary edema assessment. Left lung tissue was collected, blotted, weighed, and then placed in an oven at 80 °C for 48 h to obtain dry weight. Tissue edema was assessed by calculating the ratio of wet lung weight (W) to dry lung weight (D).

Histopathological evaluation. The right upper lobe tissues of the mice in different experimental groups were collected,

washed twice with PBS, fixed in 4% paraformaldehyde solution, and stored at 4 °C. Samples were embedded in paraffin and sliced at the same position (about 5 mm). Sections were stained with hematoxylin-eosin (H&E) and Masson, respectively, and observed and filmed under a microscope (200 × magnification, Nikon).

Immunohistochemical assessment. Tissue samples were deparaffinized in xylene. After treatment with 30% H_2O_2, sections were blocked in 5% bovine serum albumin and incubated with anti-TLR-4 or anti-MyD88 primary antibodies overnight at 4 °C. After incubation with HRP-labeled secondary antibody for 2 h, staining was performed and examined under a microscope (200 × magnification).

2.4. Acute toxicity and effect on the viability of RAW264.7 cells

A CMC-Na suspension of TAC at a maximum concentration of 0.2 g/mL was prepared, oral administration at the rate of 10 mL/kg body was given to the Kunming mice. Sixteen mice were taken and divided into 4 groups, with 4 mice in each group. The TAC treatment group mice were orally administrated with TAC suspension, with single doses of 2000, 1000, and 500 mg/kg body weight, respectively. The control group had a normal diet. After administration, external appearance including mortality, unusual developments in the skin and eyes, behavioral changes were examined (Devi, et al. 2022).

MTT assay was done as previously reported.(Shang, et al. 2021) RAW264.7 cells in logarithmic growth phase were digested with trypsin, diluted with medium to 1×10^4 cells/mL, and cultured in 96-well plate (90 μL of cell suspension per well) for 4 h. Adding TAC and DCF at different concentrations (0, 1, 3, 10, 30, and 100 μM led to three wells per concentration). These continued to culture for 20 h. Later, 15 μL of MTT (5 mg/mL, Solarbio, China) was added and incubated for another 4 h. We then removed the supernatant and added 100 μL of DMSO to each well. Samples were agitated at low speed for 10 min, and the absorbance of each well was measured at 490 nm to calculate the cell viability.

2.5. Measurement of inflammation related cytokine

Duration of tested agents and LPS treatment referred to the reported method (Bian, et al. 2021).The RAW264.7 cells in the logarithmic growth phase were digested with trypsin, and the cells were diluted to 1×10^4 cells/mL and inoculated into a 24-well plate; 400 μL of cell suspension was added to each well and incubated for 4 h. TAC (1 and 3 μM) or DCF (3 μM) were added with three replicate wells for each concentration. Cells were then cultured for another 12 h. After treatment with LPS (final concentration 1 μg/mL, Beyotime, China) for 6 h, the cells were centrifuged at 1000 r/min for 10 min at room temperature to collect the supernatant. The content of TNF-α and IL-6 was determined according to the standard operating procedure of the ELISA kit.

2.6. Western blot analysis

(Shen, et al. 2020) Cells (RAW264.7, HET293T-MyD88$^{-/-}$) in the logarithmic growth phase were digested with trypsin, and the cells were then diluted to 1×10^5 cells/mL and seeded into 6-well plates with 1 mL of cell suspension per well for 4 h. Different concentrations of TAC (1 or 3 μM, three replicate wells were set for each concentration) were added, and the culture was continued for 12 h. The RAW264.7 cells were treated with LPS (final concentration of 1 μg/mL) for 6 h. HET293T-MyD88$^{-/-}$ cells were stimulated with IL-1 β (final concentration of 10 ng/mL) for 6 h. RIPA cell lysis buffer (400 μL, containing PMSF and phosphatase inhibitor, Beyotime, China) was then added and incubated at 0 °C for 30 min, and centrifuged at 4 °C for 5 min to obtain the cytoplasmic fraction using a BCA protein detection kit (Beyotime, China, China) to measure the protein concentration. Protein samples were run on 12% SDS-PAGE and then transferred to PVDF membranes. The blots were incubated with specific primary antibodies NF-κB and c-JUN (CST, USA) overnight at 4 °C. The samples were then washed with TBST and incubated with 1:5000 dilution of HRP-conjugated secondary antibody for 1 h at room temperature. ECL developer solution (Beyotime, China) was added for imaging.

2.7. Docking study

(Xue, et al. 2022) The 3D structure of TAC was energy-optimized under the MMFF94 force field. Target protein processing used AutoDock tools to repair residues, add hydrogen atoms and remove ligands and redundant structures such as water and co-solvents. The docking of TAC with the target protein was completed using the computer-aided drug design software AutoDockVina 1.1.2. and MGLTools. Binding site analysis used PyMOL.

2.8. Statistical analysis

SPSS 20.0 software was used for analysis, and the data in the same group were expressed as mean ± standard deviation (SD). One-way comparisons between two groups were performed using the independent sample *t*-test. One-way analysis of variance (one-way ANOVA) was used for the comparison of means among multiple groups. $P < 0.05$ indicates a significant difference.

3. Results and discussion

3.1. TAC showed good anti-inflammatory activity in mice

The xylene-induced ear edema model has been widely used for screening drug anti-inflammatory activities to its easy operation and good reproducibility (Khan, et al. 2021). Thus, we adopted the xylene-induced ear edema model to evaluate the anti-inflammatory inhibition rate of TAC and DCF *in vivo* 4 h after oral administration at varying doses and times. The TAC inhibition rate against ear edema in mice ranged from 23.8% to 78.2% (2.5 to 40 mg/kg, respectively, Fig. 2A). The anti-inflammatory activity of TAC increased with increasing dose and was better than that of the control drug DCF at doses of 2.5 mg/kg, 5 mg/kg, 10 mg/kg, and 20 mg/kg. At 40 mg/kg, the anti-inflammatory activity of TAC was comparable to that of DCF. Overall, TAC anti-inflammatory performance was superior to that of DCF at low doses, and the differences were negligible when the dose was increased.

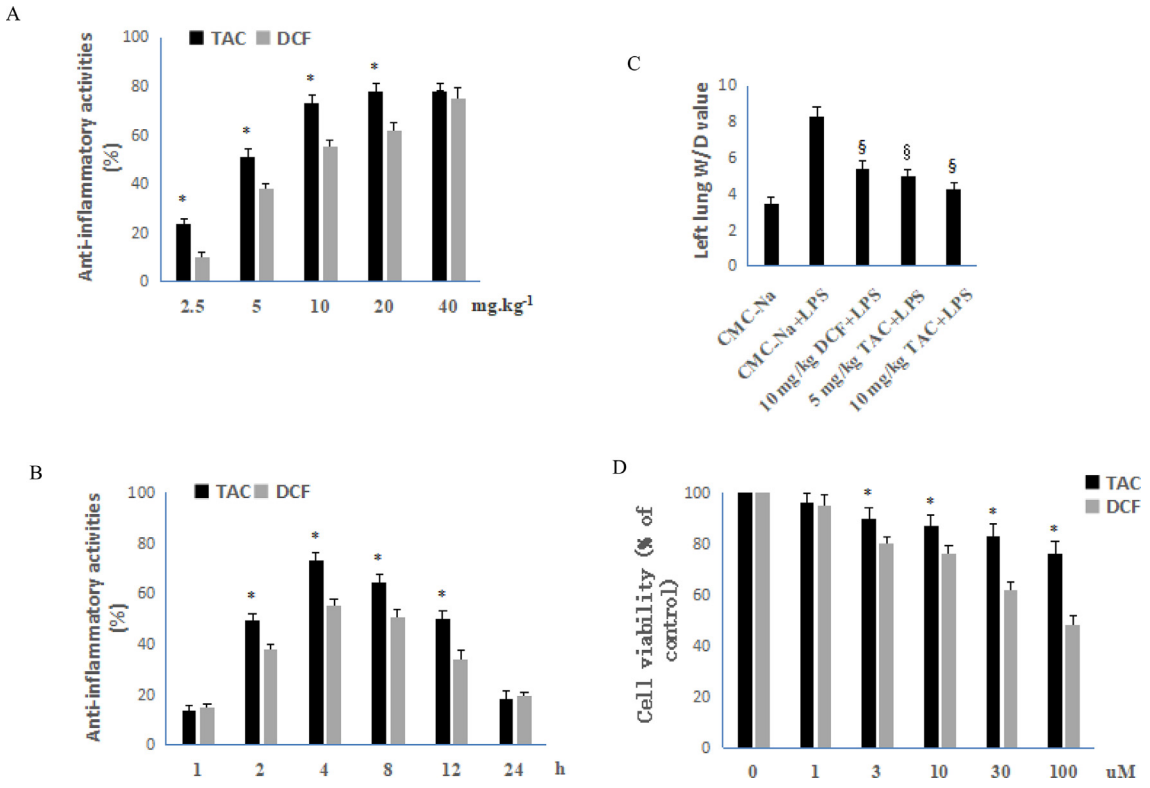

Fig. 2 Anti-inflammatory activity and cytotoxicity of TAC and DCF. A: Anti-inflammatory activity of TAC and DCF at different doses 4 h after orally administration, each column represents the mean ± SD (n = 10). B: Orally anti-inflammatory activity of TAC and DCF at the same dose of 10 mg/kg at different administration times, each column represents the mean ± SD (n = 10). C: Effect of TAC and DCF on pulmonary edema in ALI mice, each column represents the mean ± SD (n = 6). D: Effects of DCF and TAC on the cell viability of RAW264.7 cells, error bars indicate the means ± SD of three independent replicates. All comparisons were analysed with Student's *t*-test. *P < 0.05 *vs.* DCF, §P < 0.05 *vs.* placebo.

Fig. 2B shows the anti-inflammatory activities of 10 mg/kg TAC and DCF at different administration times. After 1 h of administration, the anti-inflammatory activity of TAC increased with time and reached a peak at 4 h with inhibition rate of 73.1%. This then gradually decreased, but still had a certain anti-inflammatory activity at 24 h. Compared with DCF, the activity of TAC was higher than DCF at 2 h, 4 h, 8 h, and 12 h, but the difference was not significant at other time points. The anti-inflammatory activity of TAC was still high 12 h after oral administration. This means that TAC may be used as a potential long-acting anti-inflammatory drug. We also evaluated the activity of curcumin against xylene-induced inflammation in mice at 100 mg/kg. After 4 h of administration, the inhibition rate was 21.5%, which was significantly weaker than its triazole derivative TAC.

3.2. TAC can mitigate LPS-induced acute lung injury

Induction of acute lung injury in mice by instillation of LPS offers accurate dosage, good repeatability, relatively simple detection method, clear inflammatory events, and can reflect the entire physiological process of acute inflammation; thus, it is widely used to study inflammation physiology and discover new pro-inflammatory resolution molecules (Huang, et al. 2020). During acute lung injury, the pulmonary vascular barrier is damaged resulting in a widening of the intercellular space. Fluid infiltration from the blood vessels into the interstitial space results in an increase in the weight of the lung tissue (de Oliveira, et al. 2019). Therefore, we calculated the W/D values of LPS-treated mouse lungs to observe the effect of TAC on the severity of LPS-induced pulmonary edema.

The experimental results showed that the W/D value of the placebo group was 3.5. After LPS treatment, the pulmonary edema obviously increased with a W/D value of 8.3. Fig. 2C shows that all test drug groups had lower W/D values. The left lung W/D value of 5 mg/kg TAC in ALI mice was comparable to 10 mg/kg DCF. At a TAC of 10 mg/kg, the W/D value was 4.3, and the degree of pulmonary edema was significantly reduced. In conclusion, under the dose of 5 mg/kg or 10 mg/kg, DCF can reduce the pulmonary interstitial fluid exudation and decrease the degree of pulmonary edema injury in mice.

3.3. Histopathological analysis

The weight of lung tissue increases during ALI because inflammatory cells in the blood migrate to the lung interstitium through the damaged endothelial cell, and the alveolar structure is destroyed (de Oliveira, et al. 2019). Part of the alveolar tissue is damaged and repaired abnormally, thus resulting in abnormal structure and fibrosis (Pinheiro, et al. 2019). The degree of lung tissue damage and fibrosis in ALI mice can be assessed through histopathological analysis.

H&E staining showed that the overall structure of the lung tissue of the mice in the placebo group was normal with clear alveolar structure (Fig. 3). There was no vascular congestion and dilation (black arrow) in the tissue, and no obvious inflammatory cell infiltration in the tissue. In the LPS model group, the overall lung structure was abnormal, and many alveoli were atrophied and collapsed in the tissue. The black arrow in the figure indicates many alveolar epithelial cells shed and necrotic; the tissue interstitium was congested (blue arrow). The overall structure of the lung tissue of the mice in the TAC treatment group was basically normal, the alveolar structure of the tissue was clear, the alveolar epithelial cells did not obviously fall off (black arrow), and there was no vascular congestion or expansion in the tissue interstitium. Compared with the LPS model group, the normal alveolar structure was less damaged in the TAC treatment group: The degree of alveolar cavity edema, fusion, collapse, and rupture were significantly reduced. Meanwhile, there was less exudation of inflammatory immune cells and red blood cells. Pathological changes were significantly reduced versus the LPS model group.

Image-Pro Plus 6.0 (Media Cybernetics, Inc., Rockville, MD, USA) was used for analysis of Masson-stained pictures. The same blue color was selected as the unified standard for judging the degree of positivity in all of the pictures. The tissue area, fibrous tissue area, and fibrosis rate of each photo were obtained. Masson staining showed almost no fibrosis in normal lung tissue, but the degree of fibrosis in the LPS model group was close to 10%. Compared with the LPS model group, the TAC-treated mice had a significantly lower fibrosis rate, especially at 10 mg/kg. The fibrosis rate was only 1%. These results indicate that the inflammatory and pathological indicators of LPS-induced lung injury were significantly improved in the TAC administration group. TAC can effectively reduce the degree of pulmonary fibrosis in mice with ALI. Attenuating fibrosis in ALI by pro-inflammatory resolution provides a new strategy for critically ill COVID-19 patients.

3.4. Immunohistochemistry analysis

Extensive preclinical evidence suggests that targeting the myeloid differentiation 2 (MD2), toll-like receptors 4 (TLR4), and myeloid differentiation factor 88 (MyD88) signaling pathways is an effective approach for the treatment of sepsis and ALI (-

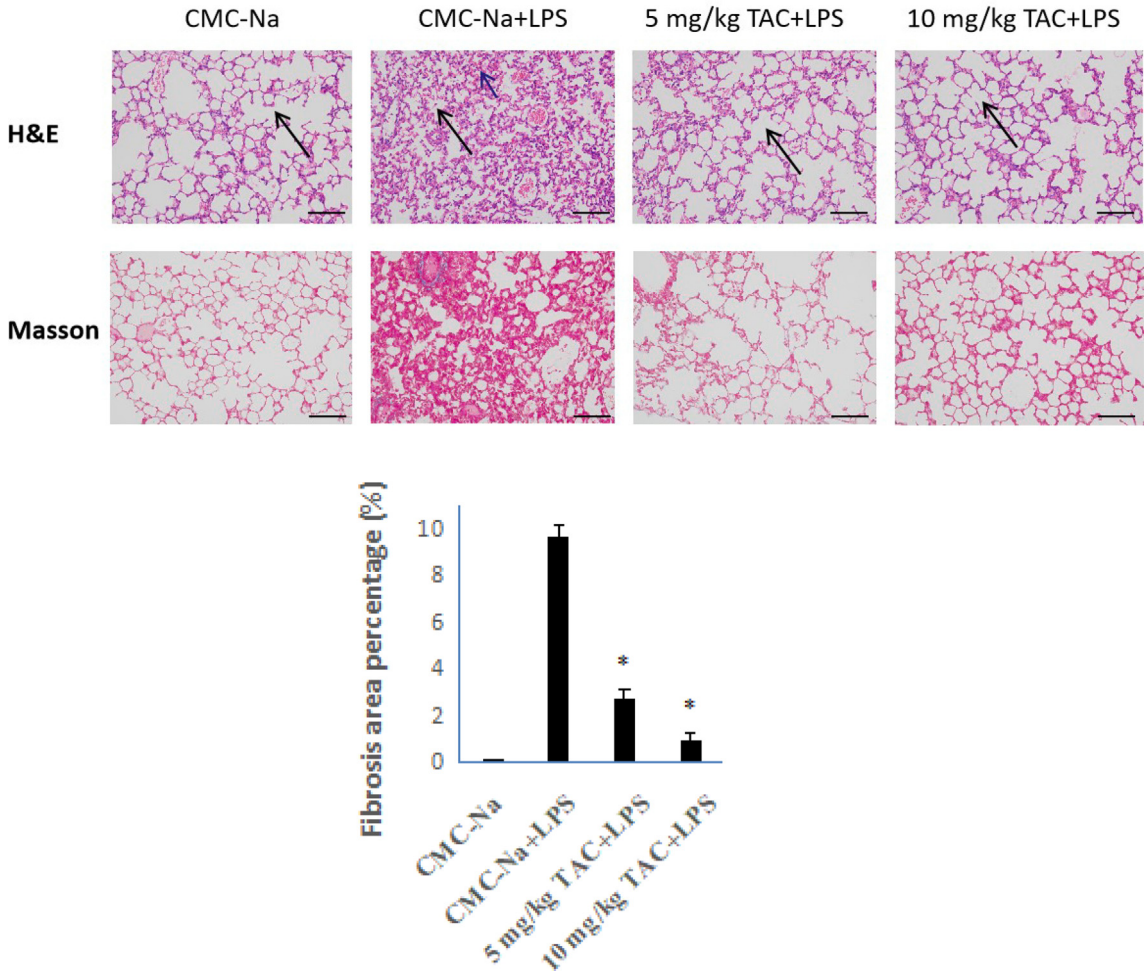

Fig. 3 HE- and Masson-stained sections of the right upper lobe of ALI mice (x 200). The histogram is the proportion of fibrous tissue obtained from the analysis of Masson-stained samples, error bars indicate the means ± SD of three independent replicates. *P < 0.05 *vs.* placebo.

Płóciennikowska, et al. 2015). The TLR superfamily plays a crucial role in host defense and inflammation. TLR4 and its accessory protein MD2 complex are the only receptors for LPS recognition. Activation of TLR4 will recruit MyD88, activate NF-κB and AP-1, and ultimately lead to the production of proinflammatory cytokines (Liu, et al. 2020). Therefore, to further study the mechanism by which TAC exerts anti-inflammatory activities, we analyzed the expression of TLR4 and MyD88 in lung cells of ALI mice by immunohistochemistry.

The immunohistochemical results are shown in Fig. 4. The TLR4 protein was mainly expressed on the normal cell membrane, and thus TLR4 protein-positive cells were seen in the placebo group. The expression of TLR4 and MyD88 proteins in the LPS group were significantly enhanced versus the placebo group. The expression levels of TLR4 and MyD88 proteins decreased after TAC treatment. This suggests that the *in vivo* anti-inflammatory effect of TAC is associated with altered expression of TLR4 and MyD88.

3.5. Acute toxicity and effect on the viability of RAW264.7 cells

The acute toxicity study of TAC showed that all Kunming mice treated with different doses were healthy, active, and showed no signs of toxicity. TAC did not show any behavioral changes in all the treated mice at the highest dose of 2000 mg/kg body weight.

The MTT assay was used to examine the effects of DCF and TAC on the viability of RAW264.7 cells. The viability of RAW264.7 cells gradually decreased with increasing DCF and TAC doses after 4 h of co-culture with different concentrations of DCF and TAC (Fig. 2D). TAC showed weaker cytotoxicity from 3 to 100 mg/kg. Especially at a dose of 100 mg/kg, the viability of RAW264.7 cells after TAC treatment was close to 80%. The results reflect the advantages of curcumin derivatives in terms of cellular safety.

3.6. TAC inhibits the of pro-inflammatory cytokine release induced by LPS

To test the *in vitro* anti-inflammatory activity of TAC, we used ELISA to detect the effect of TAC on inflammatory factors in LPS-stimulated RAW264.7 cells. Both TNF-α and IL-6 in the placebo group were present in trace amounts (Fig. 5A). The levels of TNF-α and IL-6 were significantly increased in RAW264.7 cells after 6 h of treatment with LPS. The levels of TNF-α and IL-6 in the tested drug groups were significantly decreased versus the LPS group. More specifically, there was no significant difference in the expression levels of TNF-α and IL-6 between 3 μM DCF and 1 μM TAC. After 3 μM TAC treatment, the contents of TNF-α and IL-6 in RAW264.7 cells were significantly decreased versus the same dose of DCF. The results showed that TAC could significantly reduce the cellular inflammatory storm induced by LPS stimulation. The immune system is usually over-activated in ALI, thus leading to the production of a cytokine storm. This in turn releases many inflammatory factors such as TNF, IL-6, IL-18, and IFN-γ (Soni, et al. 2016). Of these, the interleukin factors and pro-inflammatory cytokine TNF-a are considered to be the most likely biomarkers to effectively predict the development and dynamics of inflammation.

3.7. TAC targets the MD2-TLR4-MyD88 signaling pathway

The immunohistochemical results showed that TAC could affect the expression levels of TLR4 and MyD88. Activation of the TLR4-MyD88 pathway led to the production of pro-inflammatory cytokines NF-κB and AP-1 (Zhu, et al. 2020). Therefore, to further validate the effect of TAC on the TLR4-MyD88 pathway, we used Western blotting to detect the effect of TAC on the expression of NF-κB and AP-1 in RAW264.7 cells (Fig. 5B). The expression of NF-κB was significantly increased after RAW264.7 cells were incubated with LPS. For the two groups of TAC-pretreated RAW264.7 cells, the expression of NF-κB and AP-1 decreased with increasing dose. Combined with the results of immunohistochemical experiments, we see that TAC can suppress the TLR4-MyD88 signaling pathway, thus reducing the production of the pro-inflammatory cytokines NF-κB and AP-1.

To further validate the effect of TAC to the TLR4-MyD88 signaling pathway, we used IL-1β to induce HET293T-Myd88$^{-/-}$ and produce an inflammatory response. We used this to detect the expression of NF-κB. IL-1β can bind to IL-1R1 and IL-1R2, activate NF-κB signaling pathway, and induce the synthesis and expression of chemokines GRO-2 and CXCL9 (Luo, et al. 2018). As shown in Fig. 5C, the expression of NF-κB was significantly increased after incubation of HET293T-MyD88$^{-/-}$ cells with IL-1β. However, the

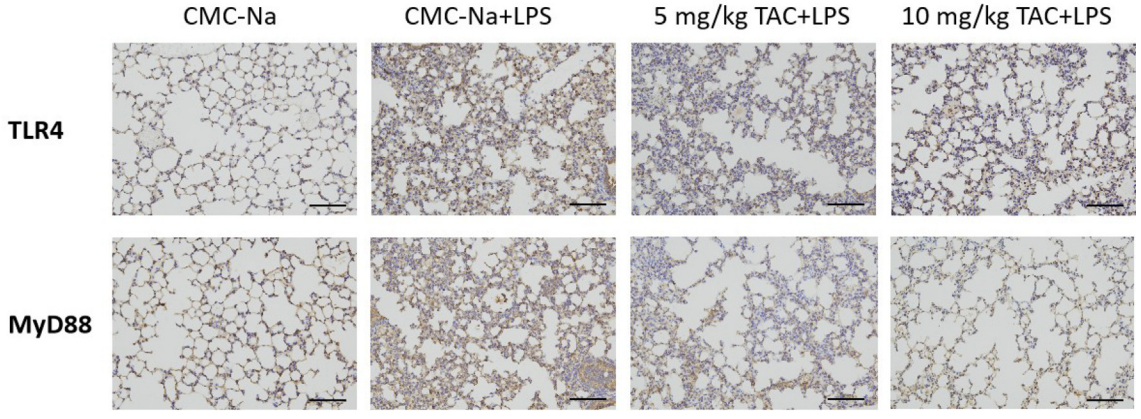

Fig. 4 Immunohistochemistry analyze the expression of TLR4 and MyD88 of the right upper lobe of ALI mice (x 200).

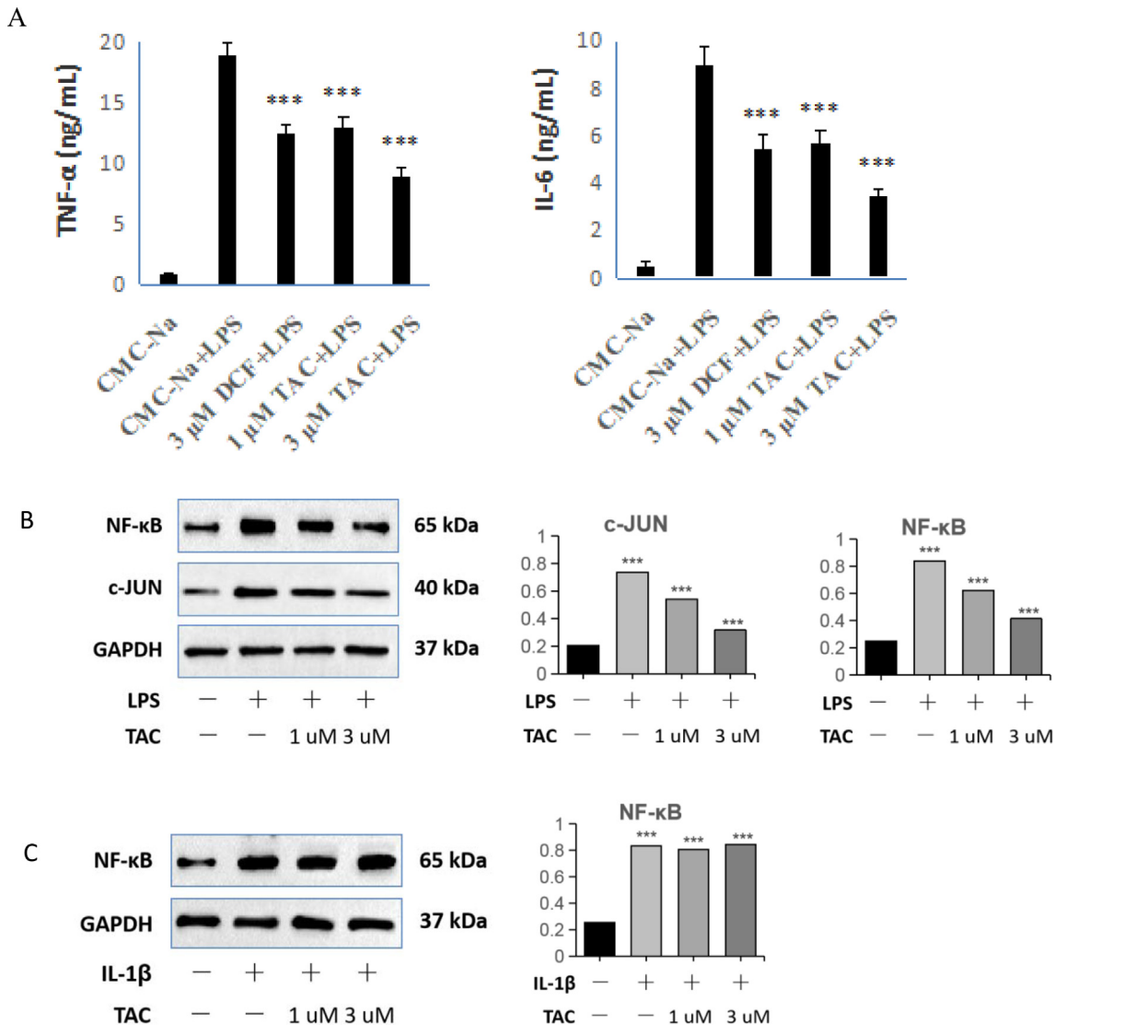

Fig. 5 Effects of TAC and DCF on LPS-stimulated RAW264.7 inflammatory factors TNF-α and IL-6 by ELISA, and effect of TAC on the expression of NF-κB and c-JUN. B: RAW264.7 cells; C: HET293T-MyD88$^{-/-}$ cells. ***p < 0.001 *vs.* control.

expression of NF-κB did not change after incubation with IL-1β in HET293T-MyD88$^{-/-}$ cells pretreated with different doses of TAC. Indeed, MyD88 is a key adaptor molecule in TLR pathway signaling transduction. Specifically blocking the self-polymerization of MyD88 can prevent the formation of Myddosome complexes and the transduction of inflammatory signaling (Zheng, et al. 2020). MyD88 gene knockout attenuates paraquat-induced acute lung injury (Shen, et al. 2017).

Curcumin can regulate inflammatory mediators and treat inflammatory diseases.by binding to TLRs and regulating downstream NF-κB, mitogenactivated protein kinases (MAPK), AP-1 and other signaling pathways (Kotha and Luthria 2019). Due to TAC retains the parent structure of curcumin, showed similar pharmacological effects. Meanwhile, curcumin can down-regulate NF-κB through acting on several pathways, such as peroxisome proliferator-activated receptor gamma (PPARγ) (Li, et al. 2019; Zhu, et al. 2019), tyrosine kinases (Golonko, et al. 2019), angiotensin II (Howell, et al. 2013), etc. Here, TAC failed to influence the expression of NF-κB in HET293T-MyD88$^{-/-}$ cells further demonstrating that TAC exerts an anti-inflammatory effect by specifically suppressing the TLR4-MyD88 signaling pathway.

3.8. Docking study

TAC can exert an anti-inflammatory activity by targeting the TLR4-MyD88 signaling pathway; thus, we selected MyD88 protein and CD2-TLR4 complex related to this signaling pathway for molecular docking studies to determine possible targets with their specific modes of action. We downloaded the co-crystal structure of the target protein from PDB, and used the docking program AutoDockVina and MGLTools to complete this work. Docking results showed that the CD2-TLR4 complex could be docked to then express a high binding affinity free energy of − 8.9 kcal/mol for TAC. As shown in Fig. 6B, TAC is incorporated in the MD2 pocket in a Y-shape. The binding model shows that TAC and LPS occupy

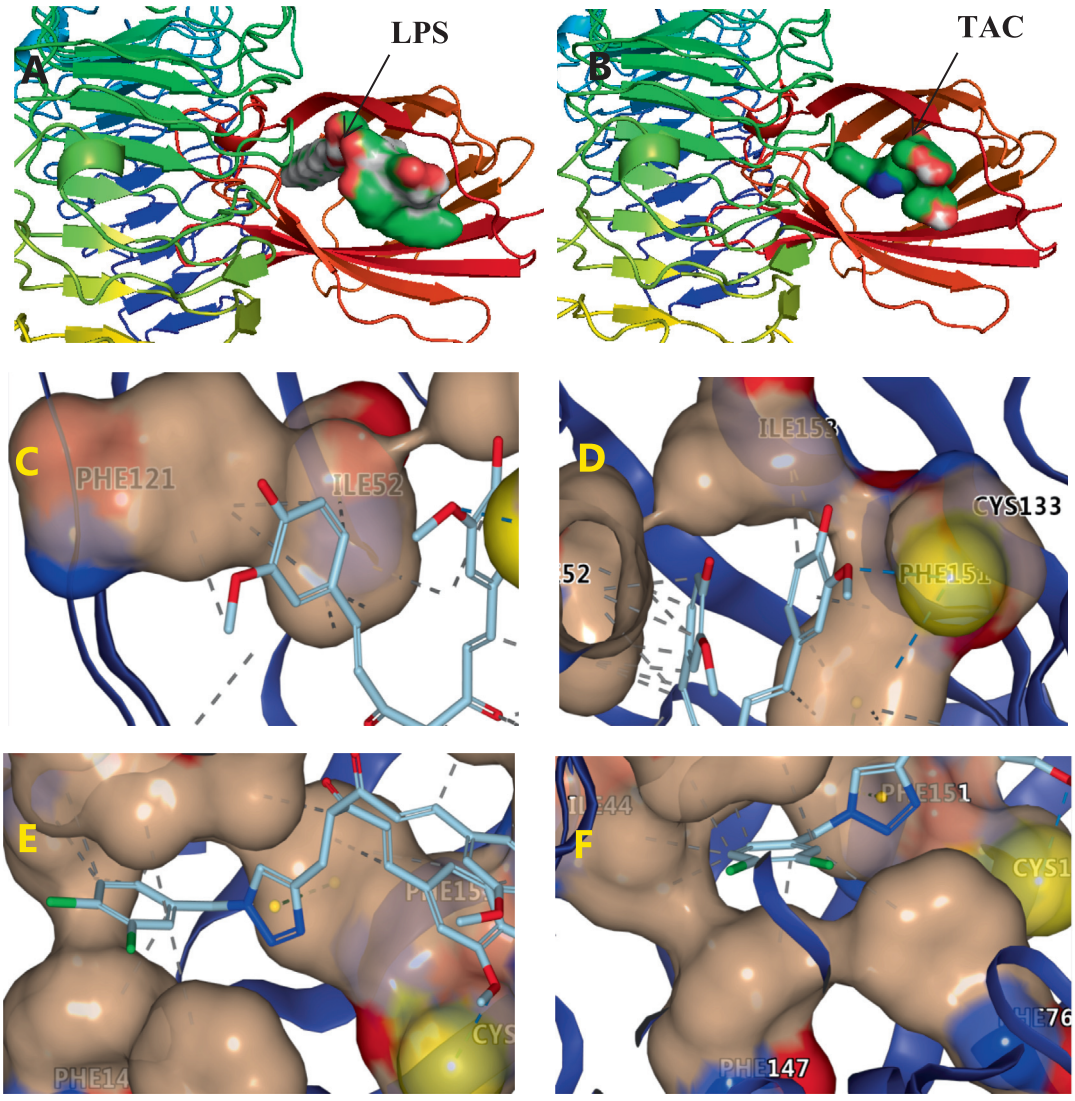

Fig. 6 Docking mode of TAC with MD2-TLR4, and co-crystallization structure of LPS-MD2-TLR4 (3FXI). A and B: Ligand is shown on the surface. C, D, E and F: Ligand is shown by licorice. —hydrophobic interaction, —hydrogen bond, —π-π stacking.

the target site of MD2-TLR4 in a similar posture. This illustrates the competitive binding ability of TAC (Fig. 6A, 6B).

Multiple β-sheets of MD2 form a large hydrophobic pocket with a total surface area of about 1000 Å (Park, et al. 2009). The inner surface of the MD2 ligand-binding pocket is largely covered by hydrophobic residues, making it suitable for binding of bulky hydrophobic ligands. One of the phenyl rings of TAC penetrates into the hydrophobic pocket of MD2 and interacts with ILE52 and PHE121 in the form of hydrophobic interactions (Fig. 6C). Another benzene ring of TAC interacts with ILE153 in the form of hydrophobic interaction. It is especially rare that the methoxy group on the benzene ring interacts with the thiol group of CYS133 through hydrogen bonding (Fig. 6D). Cys133 is the only free sulfhydryl group exposed in the hydrophobic pocket, and it can be a potential drug-binding site for inhibition of TLR4 signaling. The triazole pharmacophore interacts with PHE151 in the form of π-π stacking (Fig. 6E). This π-π stacking interaction greatly contributes to the stable docking structure. Meanwhile, the dichlorophenyl ring interacts with ILE44, ILE63, PHE76, and PHE147 via hydrophobic interactions (Fig. 6F). TAC contains unsaturated carbonyl groups, but the interaction between TAC and MD2 does not appear to involve covalent binding.

The MD2-TLR4 complex is the only receptor capable of recognizing LPS (Park, et al. 2009). The co-crystal structure of LPS-MD2-TLR4 showed that LPS binds to MD2 via several amino acid residues such as Phe-121, Phe-126, Tyr-131, and Lys-132. Molecular simulation docking results indicated that TAC and MD2-TLR4 could form key hydrogen bonds and hydrophobic interactions. Thus, TAC was thought to exert an anti-inflammatory effect by interfering with the binding of the LPS to the TLR4-MD2 complex.

4. Conclusions

In summary, this study investigated the anti-inflammatory activity of TAC and explored its possible targets. Multilevel experiments showed that TAC exhibited good anti-inflammatory activity both *in vivo* and

in vitro and could significantly inhibit LPS-induced ALI in mice. The results show that the intervention of TAC on the MD2-TLR4 pathway can effectively reduce the inflammatory response, but its specific mechanism and targets still need further study.

Funding

This research was funded by the Natural Science Foundation of Jiangsu Province, China (BK20210939).

CRediT authorship contribution statement

He WeiGang: Writing – original draft, Writing – review & editing. **Liu KaiQiang:** Data curation. **Hou XueYou:** . **Xu JiaHan:** . **Zhi TaiXin:** . **Deng YingKai:** . **Hu JunYi:** Software, Visualization, Data curation. **Jin MoYan:** Software, Visualization. **Wang JiaChen:** Software, Visualization. **Wang Xin:** Writing – original draft, Writing – review & editing. **Sun XianYu:** Writing – original draft, Writing – review & editing, Project administration, Funding acquisition.

Declaration of Competing Interest

The authors declare that they have no known competing financial interests or personal relationships that could have appeared to influence the work reported in this paper.

Acknowledgments

We thank all the technicians and faculty in the analytical facility center of the Institute of Changshu Institute of Technology.

References

Bian, M., Zhen, D., Shen, Q.K., Du, H.H., Ma, Q.Q., Quan, Z.S., 2021. Structurally modified glycyrrhetinic acid derivatives as anti-inflammatory agents. Bioorg. Chem. 107,. https://doi.org/10.1016/j.bioorg.2020.104598 104598.

Campbell, M.S., Carlini, N.A., Fleenor, B.S., 2021. Influence of curcumin on performance and post-exercise recovery. Crit. Rev. Food Sci. Nutr. 61 (7), 1152–1162. https://doi.org/10.1080/10408398.2020.1754754.

Caprioglio, D., Torretta, S., Ferrari, M., Travelli, C., Grolla, A.A., Condorelli, F., Genazzani, A.A., Minassi, A., 2016. Triazole-curcuminoids: A new class of derivatives for 'tuning' curcumin bioactivities? Bioorg. Med. Chem. 24 (2), 140–152. https://doi.org/10.1016/j.bmc.2015.11.044.

Cepkova, M., Matthay, M.A., 2006. Pharmacotherapy of acute lung injury and the acute respiratory distress syndrome. J. Intensive Care Med. 21 (3), 119–143. https://doi.org/10.1177/0885066606287045.

Coperchini, F., Chiovato, L., Ricci, G., Croce, L., Magri, F., Rotondi, M., 2021. The cytokine storm in COVID-19: Further advances in our understanding the role of specific chemokines involved. Cytokine Growth Factor Rev. 58, 82–91. https://doi.org/10.1016/j.cytogfr.2020.12.005.

de Oliveira, M.T.P., de Sá Coutinho, D., Tenório de Souza, É., Stanisçuaski Guterres, S., Pohlmann, A.R., Silva, P.M.R., Martins, M.A., Bernardi, A., 2019. Orally delivered resveratrol-loaded lipid-core nanocapsules ameliorate LPS-induced acute lung injury via the ERK and PI3K/Akt pathways. Int. J. Nanomed. 14, 5215–5228. https://doi.org/10.2147/ijn.S200666.

Deng, C.X., 2020. Glucocorticoids save lives in COVID-19 patients. Int. J. Biol. Sci. 16 (13), 2477–2478. https://doi.org/10.7150/ijbs.49125.

Devi, T.B., Jena, S., Patra, B., Singh, K.D., Chawla, S., Raina, V., Koijam, A.S., Parida, A., Rajashekar, Y., 2022. Acute and sub-acute toxicity evaluation of dihydro-p-coumaric acid isolated from leaves of Tithonia diversifolia Hemsl. A. Gray in BALB/c mice. Front. Pharmacol. 13,. https://doi.org/10.3389/fphar.2022.1055765 1055765.

Golonko, A., Lewandowska, H., Świsłocka, R., Jasińska, U.T., Priebe, W., Lewandowski, W., 2019. Curcumin as tyrosine kinase inhibitor in cancer treatment. Eur. J. Med. Chem. 181,. https://doi.org/10.1016/j.ejmech.2019.07.015 111512.

Howell, J.C., Chun, E., Farrell, A.N., Hur, E.Y., Caroti, C.M., Iuvone, P.M., Haque, R., 2013. Global microRNA expression profiling: curcumin (diferuloylmethane) alters oxidative stress-responsive microRNAs in human ARPE-19 cells. Mol. Vis. 19, 544–560.

Huang, X.T., Liu, W., Zhou, Y., Sun, M., Yang, H.H., Zhang, C.Y., Tang, S.Y., 2020. Galectin-1 ameliorates lipopolysaccharide-induced acute lung injury via AMPK-Nrf2 pathway in mice. Free Radic. Biol. Med. 146, 222–233. https://doi.org/10.1016/j.freeradbiomed.2019.11.011.

Hughes, K.T., Beasley, M.B., 2017. Pulmonary manifestations of acute lung injury: More than just diffuse alveolar damage. Arch. Pathol. Lab. Med. 141 (7), 916–922. https://doi.org/10.5858/arpa.2016-0342-RA.

Khan, J., Ali, G., Rashid, U., Khan, R., Jan, M.S., Ullah, R., Ahmad, S., Abbasi, S.W., Khan Khalil, A.A., Sewell, R.E., 2021. Mechanistic evaluation of a novel cyclohexenone derivative's functionality against nociception and inflammation: An in-vitro, in-vivo and in-silico approach. Eur. J. Pharmacol. 902,. https://doi.org/10.1016/j.ejphar.2021.174091 174091.

Kocaadam, B., Şanlier, N., 2017. Curcumin, an active component of turmeric (Curcuma longa), and its effects on health. Crit. Rev. Food. Sci. Nutr. 57 (13), 2889–2895. https://doi.org/10.1080/10408398.2015.1077195.

Kotha, R.R., Luthria, D.L., 2019. Curcumin: Biological, pharmaceutical, nutraceutical, and analytical aspects. Molecules 24 (16). https://doi.org/10.3390/molecules24162930.

Leist, S.R., Dinnon 3rd, K.H., Schäfer, A., Tse, L.V., Okuda, K., Hou, Y.J., West, A., Edwards, C.E., Sanders, W., Fritch, E.J., Gully, K.L., Scobey, T., Brown, A.J., Sheahan, T.P., Moorman, N.J., Boucher, R.C., Gralinski, L.E., Montgomery, S.A., Baric, R.S., 2020. A mouse-adapted SARS-CoV-2 induces acute lung injury and mortality in standard laboratory mice. Cell 183 (4), 1070–1085. e12. https://doi.org/10.1016/j.cell.2020.09.050.

Li, Q., Sun, J., Mohammadtursun, N., Wu, J., Dong, J., Li, L., 2019. Curcumin inhibits cigarette smoke-induced inflammation via modulating the PPARγ-NF-κB signaling pathway. Food Funct. 10 (12), 7983–7994. https://doi.org/10.1039/c9fo02159k.

Liu, M., Xie, J., Sun, Y., 2020. TLR4/MyD88/NF-κB-mediated inflammation contributes to cardiac dysfunction in rats of PTSD. Cell Mol. Neurobiol. 40 (6), 1029–1035. https://doi.org/10.1007/s10571-020-00791-9.

Luo, X., Zheng, T., Mao, C., Dong, X., Mou, X., Xu, C., Lu, Q., Liu, B., Wang, S., Xiao, Y., 2018. Aberrant MRP14 expression in thyroid follicular cells mediates chemokine secretion through the IL-1β/MAPK pathway in Hashimoto's thyroiditis. Endocr. Connect. 7 (6), 850–858. https://doi.org/10.1530/ec-18-0019.

Michels, N., van Aart, C., Morisse, J., Mullee, A., Huybrechts, I., 2021. Chronic inflammation towards cancer incidence: A systematic review and meta-analysis of epidemiological studies. Crit. Rev. Oncol. Hematol. 157,. https://doi.org/10.1016/j.critrevonc.2020.103177 103177.

Nelson, K.M., Dahlin, J.L., Bisson, J., Graham, J., Pauli, G.F., Walters, M.A., 2017. The essential medicinal chemistry of cur-

cumin. J. Med. Chem. 60 (5), 1620–1637. https://doi.org/10.1021/acs.jmedchem.6b00975.

Niitsu, T., Tsuchida, S., Peltekova, V., Engelberts, D., Copland, I., Otulakowski, G., Post, M., Kavanagh, B.P., 2011. Cyclooxygenase inhibition in ventilator-induced lung injury. Anesth. Analg. 112 (1), 143–149. https://doi.org/10.1213/ANE.0b013e3181fe4841.

Panoskaltsis, N., McCarthy, N.E., Knight, S.C., 2021. Myelopoiesis of acute inflammation: lessons from TGN1412-induced cytokine storm. Cancer Immunol. Immunother. 70 (4), 1155–1160. https://doi.org/10.1007/s00262-020-02702-9.

Park, B.S., Song, D.H., Kim, H.M., Choi, B.S., Lee, H., Lee, J.O., 2009. The structural basis of lipopolysaccharide recognition by the TLR4-MD-2 complex. Nature 458 (7242), 1191–1195. https://doi.org/10.1038/nature07830.

Pinheiro, A., Mendes, A.R.S., Neves, M., Prado, C.M., Bittencourt-Mernak, M.I., Santana, F.P.R., Lago, J.H.G., de Sá, J.C., da Rocha, C.Q., de Sousa, E.M., Fontes, V.C., Grisoto, M.A.G., Falcai, A., Lima-Neto, L.G., 2019. Galloyl-hexahydroxydiphenoyl (HHDP)-glucose isolated from Punica granatum L. leaves protects against lipopolysaccharide (LPS)-induced acute lung injury in BALB/c mice. Front. Immunol. 10 (1978). https://doi.org/10.3389/fimmu.2019.01978.

Płóciennikowska, A., Hromada-Judycka, A., Borzęcka, K., Kwiatkowska, K., 2015. Co-operation of TLR4 and raft proteins in LPS-induced pro-inflammatory signaling. Cell Mol. Life Sci. 72 (3), 557–581. https://doi.org/10.1007/s00018-014-1762-5.

Shang, F.F., Wang, J.Y., Xu, Q., Deng, H., Guo, H.Y., Jin, X., Li, X., Shen, Q.K., Quan, Z.S., 2021. Design, synthesis of novel celastrol derivatives and study on their antitumor growth through HIF-1α pathway. Eur. J. Med. Chem. 220,. https://doi.org/10.1016/j.ejmech.2021.113474 113474.

Shen, Q.K., Gong, G.H., Li, G., Jin, M., Cao, L.H., Quan, Z.S., 2020. Discovery and evaluation of novel synthetic 5-alkyl-4-oxo-4,5-dihydro-[1,2,4]triazolo[4,3-a]quinoxaline-1-carbox-amide derivatives as anti-inflammatory agents. J. Enzyme Inhib. Med. Chem. 35 (1), 85–95. https://doi.org/10.1080/14756366.2019.1680658.

Shen, H., Wu, N., Wang, Y., Guo, F., Chen, L., Zhang, Z., Jia, D., Zhao, M., 2017. MyD88 gene knockout attenuates paraquat-induced acute lung injury. Toxicol. Lett. 269, 41–46. https://doi.org/10.1016/j.toxlet.2017.01.015.

Soni, S., Wilson, M.R., O'Dea, K.P., Yoshida, M., Katbeh, U., Woods, S.J., Takata, M., 2016. Alveolar macrophage-derived microvesicles mediate acute lung injury. Thorax 71 (11), 1020–1029. https://doi.org/10.1136/thoraxjnl-2015-208032.

Tang, C., Liu, J., Yang, C., Ma, J., Chen, X., Liu, D., Zhou, Y., Zhou, W., Lin, Y., Yuan, X., 2022. Curcumin and its analogs in non-small cell lung cancer treatment: Challenges and expectations. Biomolecules 12 (11). https://doi.org/10.3390/biom12111636.

Tu, G.W., Shi, Y., Zheng, Y.J., Ju, M.J., He, H.Y., Ma, G.G., Hao, G. W., Luo, Z., 2017. Glucocorticoid attenuates acute lung injury through induction of type 2 macrophage. J. Transl. Med. 15 (1), 181. https://doi.org/10.1186/s12967-017-1284-7.

Wang, Y., Shan, X., Dai, Y., Jiang, L., Chen, G., Zhang, Y., Wang, Z., Dong, L., Wu, J., Guo, G., Liang, G., 2015. Curcumin analog L48H37 prevents lipopolysaccharide-induced TLR4 signaling pathway activation and sepsis via targeting MD2. J. Pharmacol. Exp. Ther. 353 (3), 539–550. https://doi.org/10.1124/jpet.115.222570.

Wang, Y., Wang, H., Zhang, C., Zhang, C., Yang, H., Gao, R., Tong, Z., 2019. Lung fluid biomarkers for acute respiratory distress syndrome: a systematic review and meta-analysis. Crit. Care 23 (1), 43. https://doi.org/10.1186/s13054-019-2336-6.

Xiao, K., He, W., Guan, W., Hou, F., Yan, P., Xu, J., Zhou, T., Liu, Y., Xie, L., 2020. Mesenchymal stem cells reverse EMT process through blocking the activation of NF-κB and Hedgehog pathways in LPS-induced acute lung injury. Cell Death Dis. 11 (10), 863. https://doi.org/10.1038/s41419-020-03034-3.

Xue, Q., Liu, X., Russell, P., Li, J., Pan, W., Fu, J., Zhang, A., 2022. Evaluation of the binding performance of flavonoids to estrogen receptor alpha by Autodock, Autodock Vina and Surflex-Dock. Ecotoxicol. Environ. Saf. 233,. https://doi.org/10.1016/j.ecoenv.2022.113323 113323.

Zhang, Y., Liu, Z., Wu, J., Bai, B., Chen, H., Xiao, Z., Chen, L., Zhao, Y., Lum, H., Wang, Y., Zhang, H., Liang, G., 2018. New MD2 inhibitors derived from curcumin with improved anti-inflammatory activity. Eur. J. Med. Chem. 148, 291–305. https://doi.org/10.1016/j.ejmech.2018.02.008.

Zheng, X.Y., Sun, C.C., Liu, Q., Lu, X.Y., Fu, L.L., Liang, G., Zhang, X.H., Chen, G.Z., 2020. Compound LM9, a novel MyD88 inhibitor, efficiently mitigates inflammatory responses and fibrosis in obesity-induced cardiomyopathy. Acta Pharmacol. Sin. 41 (8), 1093–1101. https://doi.org/10.1038/s41401-020-0410-x.

Zhi, T.X., Liu, K.Q., Cai, K.Y., Zhao, Y.C., Li, Z.W., Wang, X., He, X.H., Sun, X.Y., 2022. Anti-lung cancer activities of 1,2,3-triazole curcumin derivatives via regulation of the MAPK/NF-κB/STAT3 signaling pathways. ChemMedChem 17 (3), e202100676. https://doi.org/10.1002/cmdc.202100676.

Zhu, T., Chen, Z., Chen, G., Wang, D., Tang, S., Deng, H., Wang, J., Li, S., Lan, J., Tong, J., Li, H., Deng, X., Zhang, W., Sun, J., Tu, Y., Luo, W., Li, C., 2019. Curcumin attenuates asthmatic airway inflammation and mucus hypersecretion involving a PPARγ-dependent NF-κB signaling pathway in vivo and in vitro. Mediators Inflamm. 2019, 4927430. https://doi.org/10.1155/2019/4927430.

Zhu, G., Cheng, Z., Huang, Y., Zheng, W., Yang, S., Lin, C., Ye, J., 2020. MyD88 mediates colorectal cancer cell proliferation, migration and invasion via NF–κB/AP–1 signaling pathway. Int. J. Mol. Med. 45 (1), 131–140. https://doi.org/10.3892/ijmm.2019.4390.